Available online at www.sciencedirect.com
ScienceDirect
Ocean Engineering 34 (2007) 1225–1234
OCEAN ENGINEERING
www.elsevier.com/locate/oceaneng

Hydrodynamic tests on a plate in forced oscillation

K. Klaka[a,*], J.D. Penrose[a], R.R Horsley[a], M.R. Renilson[b]

[a]Centre for Marine Science and Technology, Curtin University of Technology, GPO Box U1987, Perth, W A 6845, Australia
[b]Centre for Marine Technology, QinetiQ, Gosport PO12 2AG, UK

Received 15 February 2006; accepted 29 June 2006
Available online 13 December 2006

Abstract

The forces and moments acting on an oscillating plate at inflow angles at or below stall are well understood. However, there is a shortage of data on surface-piercing plates undergoing rotational oscillation. A set of experiments was conducted on a series of flat plates undergoing forced rotational oscillation in calm water. The impetus for the experiments was an investigation into the hydrodynamics of sailing yacht keels, but the results may be of value for a wide range of engineering problems. The experiments showed that the two-dimensional case was not representative of three-dimensional flow conditions. There was a possible region of transitional flow for the plate in two-dimensional flow, not evidenced in the results for three-dimensional flow. The total roll moment, roll inertia, roll drag and sway force coefficients showed an inverse square root relationship to aspect ratio, with a very weak dependency on oscillation frequency and angle amplitude. Under-plate clearance effects were small for the clearance values investigated.

Keywords: Hydrodynamics; Free-surface flow; Vortical flow

1. Introduction

1.1. Background

An investigation into the roll motion of sailing yachts determined that the hydrodynamic moments exerted by the keel and rudder formed a significant contribution to the total roll moment. Preliminary work indicated that these appendages could be considered as flat plates oscillating in rotational motion. In order to investigate further, a set of experiments was conducted with a series of flat plates undergoing forced rotational oscillation in calm water. The aims of the experiments were to:

- measure the hydrodynamic roll moment and sway force acting on flat plates oscillating in calm water,
- determine the effect of plate profile shape and aspect ratio on hydrodynamic moments,
- investigate the influence of under-plate clearance and
- identify the effect of oscillation frequency and amplitude on hydrodynamic moments.

*Corresponding author. Tel.: +61 8 9266 7543; fax: +61 8 9266 4799.

0029-8018/$ - see front matter © 2006 Elsevier Ltd. All rights reserved.
doi:10.1016/j.oceaneng.2006.06.009

1.2. A note on terminology

The axes and motions used followed naval architecture practice, as a consequence of the original reason for the investigation. Sway is horizontal lateral displacement perpendicular to the axis of rotation and roll is angular displacement about the axis of rotation. The origin was on the plate centreline at the still water level and a right-handed axes convention was used.

The profile geometry of the plate is also described in terms appropriate to a yacht keel. The span may be considered the same as the depth for an upright keel and the chord equivalent to the width (Fig. 1). The geometric aspect ratio is defined for these rectangular plates as the ratio of span to chord.

1.3. Previous work

A review of the literature revealed a dearth of experimental data on forces and moments generated by flat plates in three-dimensional flow undergoing rotational oscillation at various water depths.

One of the earliest comprehensive experiments on oscillating flat plates (Keulegan and Carpenter, 1958) was

Nomenclature

A	plate profile area, m^2
AR	geometric aspect ratio, dimensionless
Cp	centre of pressure, dimensionless
C_d	drag coefficient, dimensionless
C_{dy}	appendage sway drag coefficient, dimensionless
C_m	inertia coefficient, dimensionless
C_{my}	appendage sway inertia coefficient, dimensionless
C_φ	total roll moment coefficient, dimensionless
D	representative length, m
f	force per unit length across the flow, $N\,m^{-1}$
Fn	Froude number, dimensionless
F_y	sway force, N
g	acceleration due to gravity, $m\,s^{-2}$
h	distance from plate tip when vertical, to bottom of channel, m
KC	Keulegan–Carpenter number, dimensionless
k_i	equation of motion coefficient
M	roll moment (torque) generated by plate, N m
Re	Reynolds number, dimensionless
s	span, m
T	period, s
u	instantaneous local fluid particle velocity at the surface of the object, $m\,s^{-1}$
U	velocity amplitude at plate tip, $m\,s^{-1}$
UKC	dimensionless under-plate (keel) clearance, dimensionless
V	reference velocity, $m\,s^{-1}$
w	dimensionless frequency, dimensionless
v	kinematic viscosity, $m^2\,s^{-1}$
φ_t	instantaneous roll angle, rad
φ	roll angle amplitude, rad
ρ	fluid density, $kg\,m^{-3}$
$\sigma_{C\varphi}$	standard deviation of C_φ, dimensionless
ω	radial frequency, $rad\,s^{-1}$

conducted in a small basin in which a standing wave was generated. The experiments were conducted both on circular cylinders and flat plates, all of quite small size-cylinder diameter and plate span of the order 0.1 m. The plate was stationary and the flow motion was approximately normal to the plate. The plates and cylinders were submerged at least three diameters below the free surface. The results were analysed to yield inertia and drag coefficients sufficiently accurate to show the importance of Keulegan–Carpenter number (KC) for the first time.

Another technique is to place a plate or cylinder in a U tube and then vary the oscillation amplitude at constant frequency so as to generate a linear oscillation of the flow (Bearman et al., 1985; Sarpkaya and O'Keefe, 1995). There is no free surface effect in the working part of the U tube. Their results yielded good agreement with the work of Ridjanovic (1962).

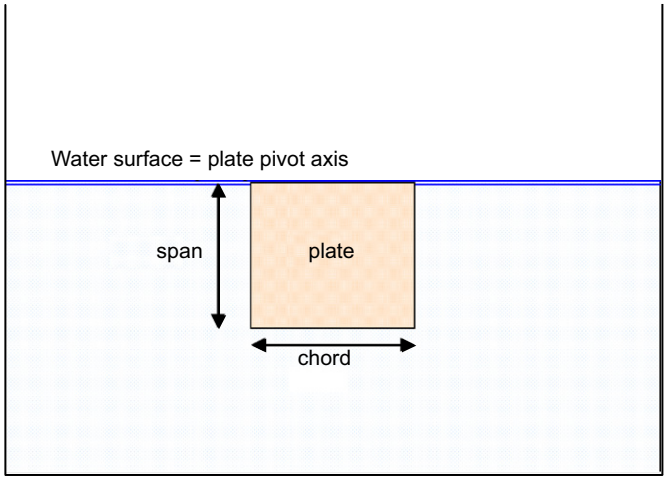

Fig. 1. Plate geometry definitions.

Ridjanovic (1962) conducted tests on a series of flat plates of varying aspect ratio. They were suspended a long way below a pivot, and connected to a pendulum. The pendulum was displaced and the hydrodynamic force determined from the angle decay rate. The plates therefore underwent a combination of linear and rotational motion. The analysis was conducted using an energy balance approach to the curve of declining angle. This yielded drag coefficients but not inertia coefficients. His drag coefficients were in general agreement with those of Sarpkaya and O'Keefe (1995).

During the 1990s Yeung developed a computational method for estimating the forces on a rotating oscillating plate pivoting at the free surface and conducted validation experiments (Yeung et al., 1997, 1998). They showed that there is a critical condition where the flow pattern changes from symmetric to asymmetric for oscillating flow normal to a flat plate in two-dimensional flow. The symmetry is in relation to the flow pattern during the initial swing (first half-oscillation) and the return swing (second half-oscillation) of a full oscillation. Both the computations and the experiments showed symmetric flow for a KC of 7.1 and asymmetric flow for KC of 13.7. Unfortunately, Reynolds number (Re) was not kept constant, therefore it is not clear whether the governing parameter is KC or Re. These experiments were only conducted for two-dimensional flow conditions and the computational method used (the free surface random vortex method) was only applicable to two-dimensional flow.

Accordingly, emphasis in the present work was directed to generating data on three-dimensional flow around a

plate undergoing angular oscillation, in the presence of a free surface.

2. Methodology

2.1. Scaling

The plate forces are a function of both Reynolds number (*Re*) and *KC*,

$$Re = \frac{VD}{v}, \tag{1}$$

$$KC = \frac{VT}{D}, \tag{2}$$

where V is the reference velocity, T is the period of oscillation, v is the kinematic viscosity and D is the representative length.

Where free surface gravity waves are present, the Froude number (*Fn*) is also influential,

$$Fn = \frac{V}{\sqrt{gD}}. \tag{3}$$

The choice of representative velocity V and length D depends on the nature of the problem under investigation. For the present work, the span s was considered a representative length, and the velocity amplitude at the tip U was used as the representative velocity V. For a flat plate pivoting along its top edge and oscillating sinusoidally, the reference velocity is then

$$V = U = \varphi\omega s, \tag{4}$$

where φ is the roll angle amplitude, ω is the radial frequency and s is the span. From Eq. (1) this yields a *Re* of

$$Re = \frac{\varphi\omega s^2}{v}. \tag{5}$$

A slightly different problem arises when considering appropriate quantities for *KC* number. Applying the chosen reference length and velocity to Eq. (2),

$$KC = \frac{2\pi s\varphi}{sT}\,T = 2\pi\varphi. \tag{6}$$

This does not relate the *KC* to the frequency of oscillation; instead, a dimensionless frequency must be used. A Froude-based frequency scaling was used, using the plate span as the reference length:

$$w = \omega\sqrt{\frac{s}{g}}, \tag{7}$$

where w is the dimensionless frequency and ω is the radial frequency of oscillation.

Forces and moments were non-dimensionalised as follows:

$$C_y = \frac{F_y}{\frac{1}{2}\rho A U^2}, \tag{8}$$

$$C_\varphi = \frac{M}{\frac{1}{2}\rho A U^2 s}, \tag{9}$$

where F_y is the sway force, M is the roll moment, A is the plate profile area, ρ is the water density, U is the maximum velocity at the plate tip and s is the plate span. The dimensionless numbers used for scaling force and moment coefficients were therefore roll amplitude φ and dimensionless frequency w.

The parameter space investigated is shown in Table 1. Four plates of different aspect ratio were tested (see Table 2 for details). Plate 1 was configured to represent two-dimensional flow conditions, enabling comparisons to be made with the work of Yeung described earlier. Plates 2–4 were representative of the aspect ratios of yacht appendages, which provided the primary motivation for the investigation.

2.2. Inertia and drag coefficients

The forces on an object in oscillatory viscous flow may be considered to comprise an inertial component, proportional to acceleration, and a drag component, proportional to velocity squared. In offshore engineering this delineation is described by the Morison equation for a stationary object in oscillating flow (Keulegan and Carpenter, 1958):

$$f = C_m\rho\frac{\pi}{4}D^2\frac{\partial u}{\partial t} + C_d\frac{\rho}{2}D|u|u, \tag{10}$$

Table 1
Parameter space constraints

Parameter	Range	
	From	To
φ (rad)	0	0.35
W	0.15	2.0
Re	2.9×10^2	1.8×10^5

Table 2
Plate geometry

	Plate 1(2-D)	Plate 2	Plate 3	Plate 4
Mass (kg)	0.105	0.075	0.151	0.069
Immersed span (m)	0.042	0.091	0.20	0.20
Chord (m)	0.294	0.10	0.10	0.0455
Area (m^2)	0.0123	0.0091	0.02	0.0091
Geometric aspect ratio	0.143	0.91	2	4.4

where f is the force per unit length across the flow, C_m is the inertia coefficient, C_d is the drag coefficient, D is the representative length, u is the instantaneous local fluid particle velocity at the surface of the object and ρ is the fluid density.

The equation of motion for a plate undergoing forced angular oscillation may be written as

$$M = k_1\ddot{\varphi}_i + k_2\dot{\varphi}_i|\dot{\varphi}_i|, \quad (11)$$

where M is the moment generated by plate, φ_i is the instantaneous roll angle, $\dot{\varphi}_i$ is the instantaneous roll angular velocity, $\ddot{\varphi}_i$ is the instantaneous roll angular acceleration and k_i are the coefficients of the equation of motion.

There are several ways of computing the equation coefficients k_1 and k_2, the method chosen here being the least-squares technique from Chakrabarti (1987, p. 192). The relationship between the coefficients k_1 and k_2 of the motion equation, and the inertia and drag coefficients of the Morison equation are readily determined for a chosen reference length and velocity.

3. Equipment and procedure

The facility used was a circulating open-water channel, with a 10 m long working length of cross-section 300 mm square. The ends of the channel were blocked off for these experiments and the channel filled with water to the desired level.

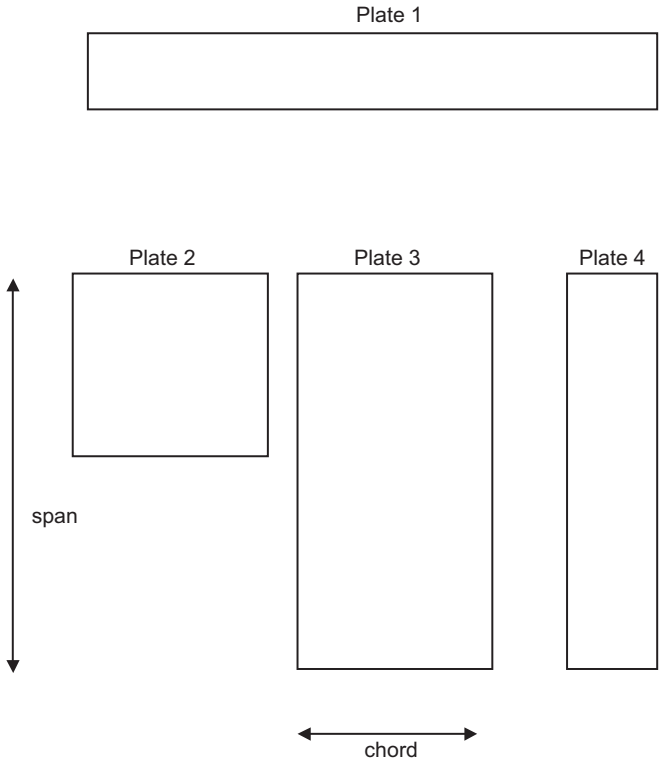

Fig. 2. Plate profiles.

The plates were made of 6 mm Perspex with square edges (Fig. 2). The plate dimensions are shown in Table 2. The flow round Plate 1 was effectively two dimensional (i.e. zero aspect ratio) in that there was a gap of only 3 mm at each end between the plate and the channel wall, which restricted flow around the ends of the plate.

The attachment rig for holding the plates comprised two horizontal aluminium base plates connected by vertical rods (Figs. 3 and 4). The upper base was clamped to the sides of the channel. The hinge supports, crank and crank arm were attached to the lower base. The lower base could be moved up and down relative to the upper base to enable tests to be conducted at different water depths while keeping the plate hinge at the static water level. The hinge supports could be adjusted transversely to accommodate plates of varying width (chord). The plate was connected to a crank arm and electric motor, the speed of which was controlled in analogue form from the power supply. The crank arm could be altered to yield different angle amplitudes.

The instrumentation for these experiments comprised 12 strain gauges on the hinge supports and crank arm attachment and a rotary potentiometer to measure the position of the crank attachment. The strain gauge configuration enabled the sway force and roll moment to

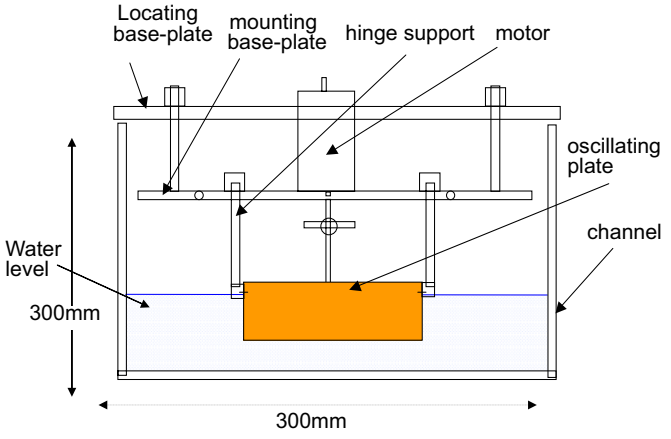

Fig. 3. End view of rig.

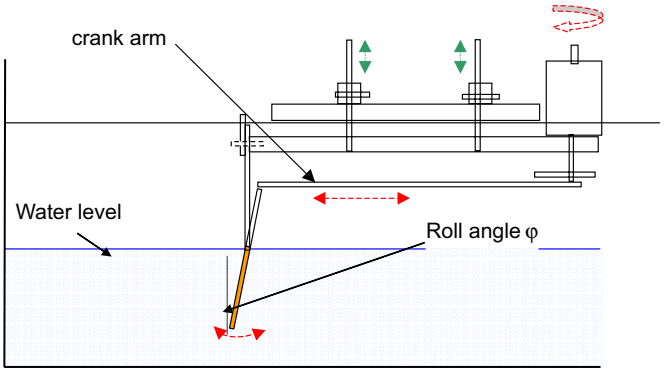

Fig. 4. Side view of rig.

be determined. The strain gauges were calibrated statically by applying known loads to each hinge support and the crank arm connection, for a number of directions over a range of amplitudes. The mean value of the gauges over typically 5 s was recorded. These mean values were plotted and a linear regression of load against voltage performed in order to determine the calibration factor. Cross-axis sensitivity of the gauges was measured during calibration and showed that measured strains were parallel to the plane of the tank.

All signals acquired were analogue voltages, digitised at 100 Hz with anti-aliasing filters set at 20 Hz. Data acquisition was limited to 20 s duration by the time taken for any generated waves to be reflected from the tank ends back to the plate.

The hydrodynamic forces and moments were required as a function of time. The total forces and moments measured comprised contributions from hydrodynamic effects, hydrostatic buoyancy, equipment inertia and bearing friction. These latter two had to be removed from the total signal in order to isolate the hydrodynamic effects. In-air measurements were modelled as a Fourier series then subtracted from the in-water measurements to remove the components due to buoyancy and equipment inertia. The analytically derived friction correction was then applied.

4. Results and discussion

4.1. Errors

Only dynamic measurements of strain were required, so problems with slowly varying strain gauge offsets were not important except for the calibration process. The physical size of the rig components was small relative to the size of the gauges, so there were errors due to strain gradients, gauge thickness etc. However, these were largely accounted for in the calibration process. The coefficients of determination for the calibration factors were always greater than 0.999. Temperature effects were accounted for firstly by using gauges with a thermal expansion coefficient similar to that of the attachment plate; secondly, by taking measurements over short duration, which were thus unlikely to experience significant change in temperature in such a large body of water. The specifications of the gauges were such that changes in signal due to thermal effects were less than 0.1%.

An object placed in a channel will experience different forces compared with the same object placed in unrestricted flow. This effect is known as blockage and is reasonably well understood for wind tunnel and towing tank experiments (Rae and Pope, 1984; Scott, 1976). However, wind-tunnel blockage corrections do not apply to tests with a pressure-relieving free surface, and towing-tank blockage corrections are largely focussed on surface wave effects and small ratios of model cross-sectional area to tank cross-sectional area. Given the uncertainty in estimating blockage effects for the current experiment, the results were left uncorrected. This should be borne in mind when comparing with experiments conducted in facilities with different model: tank cross-sectional area ratios.

Table 3
Error estimates

Plate:	1	2	2	2	3	4
w	0.77	0.42	0.78	1.33	0.81	0.84
$\sigma_{C\varphi}/C_{\varphi}$ (%)	6.7	6.9	4.7	4.1	7.8	8.1

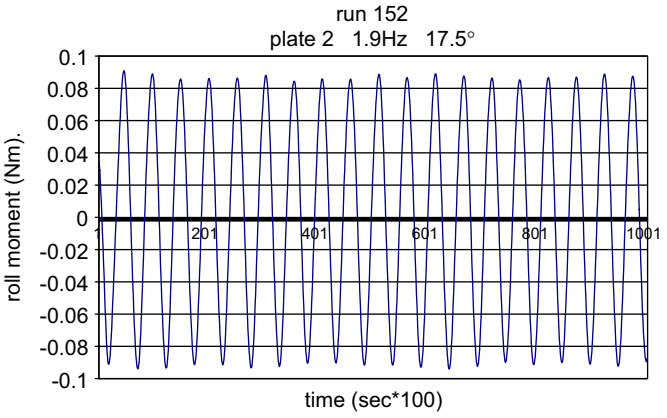

Fig. 5. Typical total roll moment as a function of time.

A summary of error magnitudes for roll moment is given in Table 3; sway force errors were of similar size. The percentage errors are similar for inertial, drag and total roll moment coefficients. The error estimates include the effect of amplitude variation evident in Fig. 5.

4.2. General observations

The results shown in this paper were selected as a representative sample of the whole data set, in the interests of brevity and clarity of presentation. Trends evident in the roll moment were reflected in the sway force. Roll angle amplitudes quoted are nominal values; they varied slightly with frequency and plate size.

A typical time domain output of total hydrodynamic roll moment is shown in Fig. 5. It exhibits an approximately sinusoidal wave form of consistent frequency and reasonably consistent amplitude. The standard deviation of the signal about the mean was used as a measure of magnitude.

The validity of applying the Morison equation to the analysis procedure was investigated. The Morison equation assumes just two components: an inertial term proportional to acceleration and a drag term proportional to the square of the velocity. It is possible that other terms were present. In order to investigate this a third component was added to the motion Eq. (11), a drag term linearly proportional to velocity. This linear drag term showed strong dependence on angle amplitude while the corresponding quadratic term varied considerably with both angle amplitude and frequency, and was for the most part a

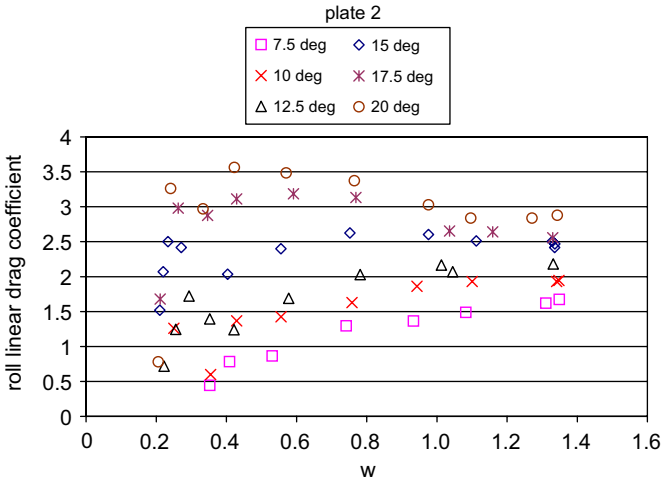

Fig. 6. Linear drag coefficient for a 3-term model.

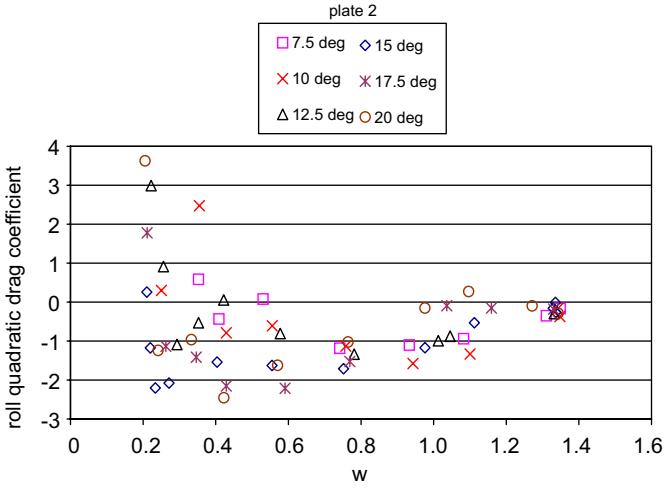

Fig. 7. Quadratic drag coefficient for a 3-term model.

negative quantity (Figs. 6 and 7). It was difficult to reconcile these results with the rationale underlying a three-component equation so it was concluded that the addition of a linear drag term was not justified.

4.3. Comparison with other work

The tests on plate 1 may be compared with the experimental work of Yeung et al. (1997) on a plate of similar shape but approximately eight times larger. Aside from the effect of Reynolds number change, the scaling of the results depends on the relative contributions of the inertial and drag terms—the inertial term is proportional to angle amplitude whereas the drag term is proportional to angle amplitude squared. Using an assumption of linearity, the results of Yeung et al. at 10° amplitude were scaled to the current results at the nearest angle amplitudes and compared in Table 4.

The Yeung data were lifted from small-scale graphs in the published paper and hence subject to processing errors

Table 4
Comparison of Yeung et al. (1997) results for 2-D plate

$w = 0.555$	Yeung et al. (1997)	Current work
$\varphi = 7.5°$, total roll moment (Nm)	0.003	0.0028
$\varphi = 12.5°$, total roll moment (Nm)	0.005	0.0049
$\varphi = 12.5°$, sway force (N)	0.121	0.093

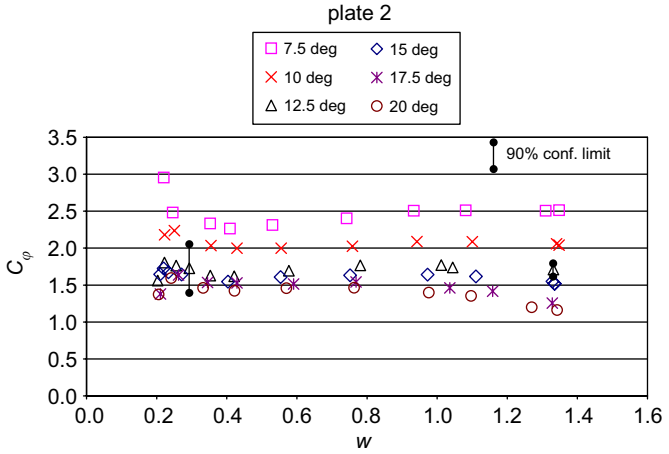

Fig. 8. Total roll moment coefficient as a function of dimensionless frequency, plate 2.

of approximately ±15%. The close agreement on roll moment was therefore considered coincidental. The 23% difference in sway force may have been due to a combination of Reynolds number effects and the scaling assumptions used. Given that there were other differences between conditions for the two sets of experiments (plate thickness, end gap, etc.) the level of agreement was considered acceptable for the purposes of validation, though questions remain regarding any direct comparison between the two data sets.

4.4. Influence of oscillation frequency

For the plates exhibiting three-dimensional flow (plates 2–4) the total roll moment coefficient was found to be largely independent of oscillation frequency for most of the conditions tested i.e. the moment was proportional to the square of the velocity at constant amplitude (Figs. 8–10).

The inertia coefficients for plates 2–4 were largely independent of frequency (Fig. 11) and the drag coefficients increased weakly with frequency (Fig. 12).

The quadratic behaviour of total roll moment with respect to frequency for plates 2–4 was not exhibited by plate 1 (Fig. 13). There was considerable structure in the moment–frequency relationship for plate 1, with a transitional zone at a frequency of 2 Hz ($w = 0.8$) indicated. Both the inertia and drag coefficients for plate 1 (Figs. 14 and 15)

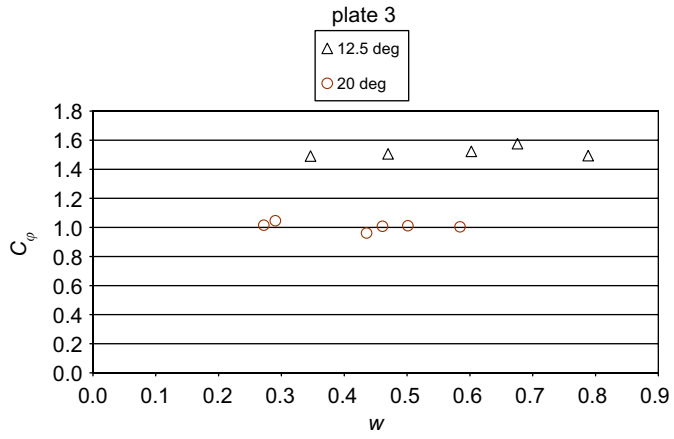

Fig. 9. Total roll moment coefficient as a function of dimensionless frequency, plate 3.

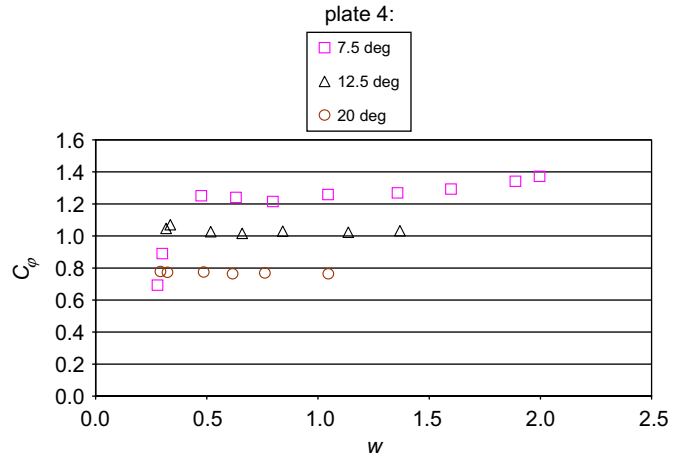

Fig. 10. Total roll moment coefficient as a function of dimensionless frequency, plate 4.

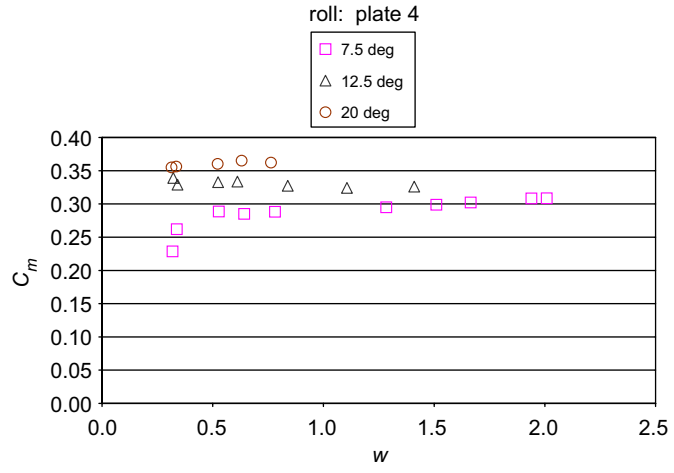

Fig. 11. Roll inertia coefficient as a function of dimensionless frequency, plate 4.

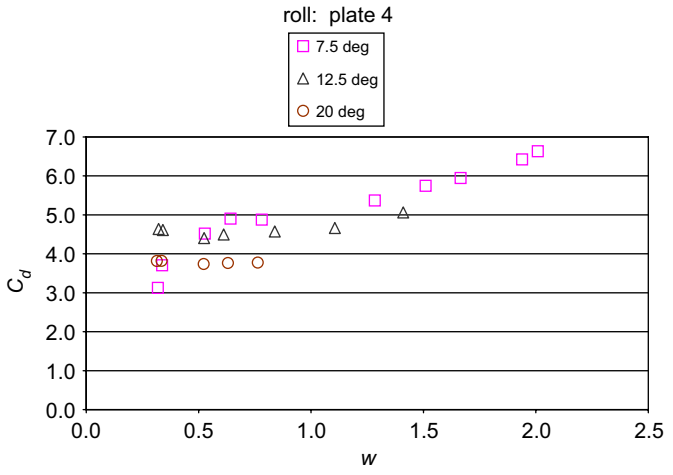

Fig. 12. Roll drag coefficient as a function of dimensionless frequency, plate 4.

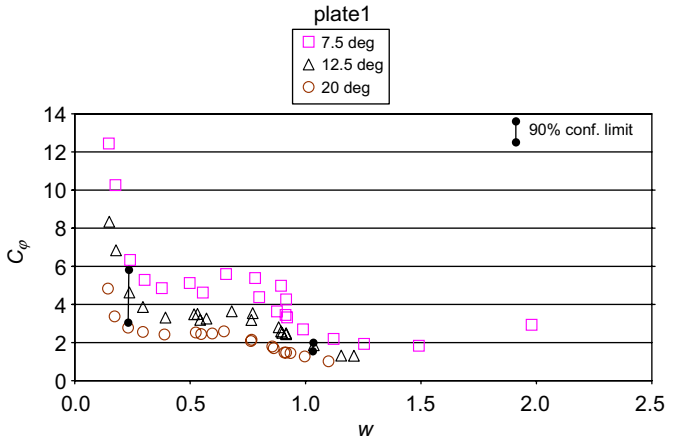

Fig. 13. Total roll moment coefficient as a function of dimensionless frequency, plate 1.

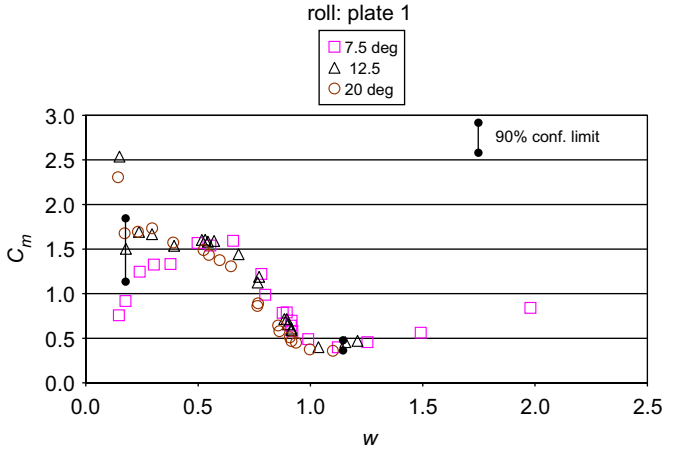

Fig. 14. Roll inertia coefficient as a function of dimensionless frequency, plate 1.

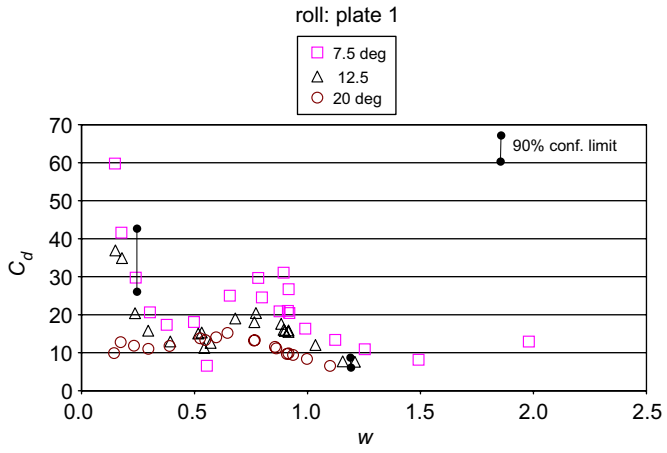

Fig. 15. Roll drag coefficient as a function of dimensionless frequency, plate 1.

also showed this transitional phase. Possible explanations for the phenomenon include:

A mechanical resonance in the rig: This would explain why the effect occurred at the same driving frequency for all angle amplitudes. However, there was no discernible energy at this frequency for tests conducted on this plate at other driving frequencies.

Wave induced resonance: This would require very short wavelengths, such as might occur in resonance across the tank. However, no transverse waves were observed and any such waves would also have been present in the experiments on the other plates.

A transition between two flow regimes: Transitional flows are to be found in other hydrodynamic scenarios such as the flow along a flat plate changing from laminar to turbulent boundary layer, or the onset of ventilation in a surface-piercing foil. The poor repeatability of results in this transition region was indicative of a transitional phenomenon. Yeung and others have discovered that two types of vortex shedding may exist for a two-dimensional oscillating plate—symmetric and asymmetric—depending on the speed of movement of the plate through the water. This change in vortex pattern is considered to be the most likely cause of the transitional phenomenon.

4.5. Influence of angle amplitude

It was not practicable to generate cross plots of coefficients against angle amplitude at constant frequency because it was not possible to set the motor speed at exactly repeatable values. Therefore, a curve-fitting procedure would be required, which would need to use data points weighted in relation to the varying error limits with frequency. The result would be more likely to show the effect of the chosen data processing technique used rather than any hydrodynamic phenomenon. Nevertheless the influence of angle amplitude can be discerned from Figs. 8 to 12. There was a general trend towards lower total roll moment coefficient with increasing angle amplitude. The inertia and drag coefficients did not show any clear trends.

4.6. Effect of under-plate clearance

The under-plate clearance was defined as

$$UKC = \frac{h}{s}, \tag{12}$$

where h is the distance from the tip of the plate when vertical, to the bottom of the channel, and s is the plate span. The UKC is usually expressed as a percentage.

The effect of under-plate clearance on total roll moment for plate 4 is shown in Fig. 16 to be very small. Similar trends were evident for plate 3 and for the sway force for the range of angles tested. The influence of under-plate clearance on inertia and drag coefficients was also similar. There was a very slight increase in roll moment at 2.5% UKC but no significant difference in roll moment between 15% and 27% UKC. Plates 1 and 2 could not be mounted low enough to conduct tests at less than 100% UKC, so effects of under-plate clearance were not investigated for them.

4.7. Effect of aspect ratio

The total roll moment coefficient for plates 2–4 showed a relationship to plate geometry (Fig. 17) for which the following model yielded an empirical fit:

$$C_\varphi = 0.727\mathrm{AR}^{-0.5}\varphi^{-0.5}, \tag{13}$$

where C_φ is the total roll moment coefficient, AR is the geometric aspect ratio and φ is the roll angle amplitude.

The relationship between inertia coefficient and plate geometry for plates 2–4 (Fig. 18) was modelled using

$$C_\mathrm{m} = 1.1(\mathrm{AR})^{-0.5}\left(\varphi^{0.25}\right), \tag{14}$$

which fitted with a variance-weighted coefficient of determination (r^2) of 0.899 over all three plates.

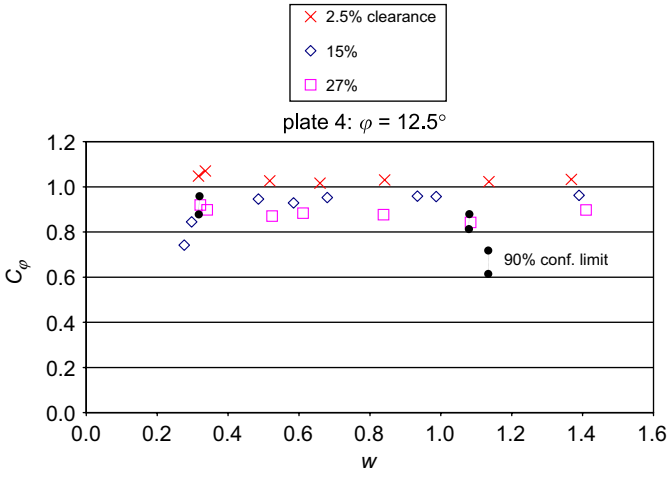

Fig. 16. Effect of under-plate clearance on total roll moment coefficient.

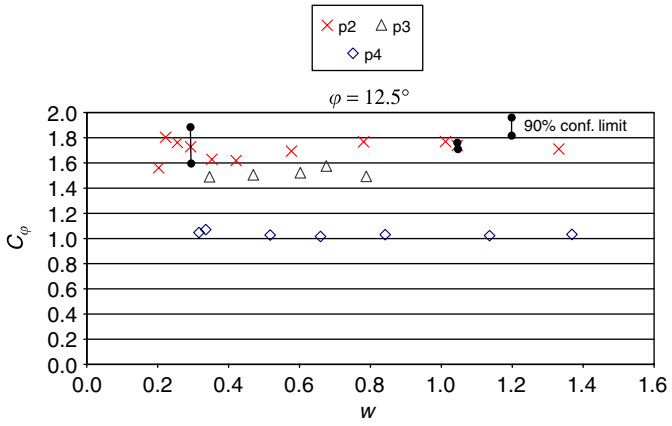

Fig. 17. Total roll moment coefficient at 12.5° amplitude.

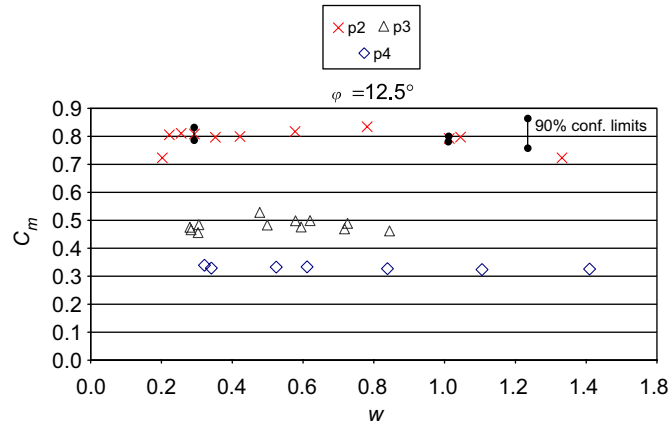

Fig. 18. Roll inertia coefficient at 12.5° amplitude.

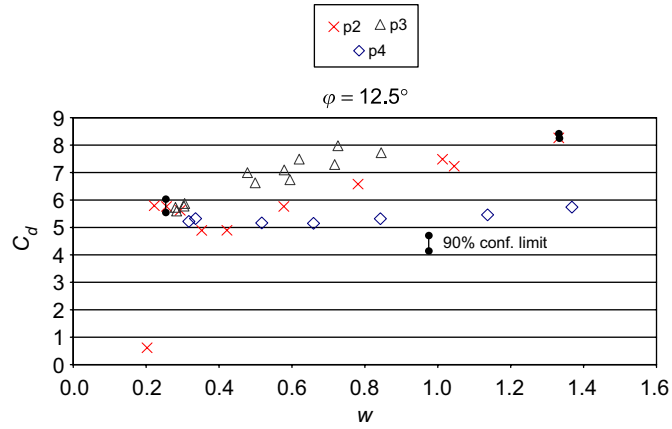

Fig. 19. Roll drag coefficient at 12.5° amplitude.

The drag coefficient was inconsistent in its behaviour (Fig. 19), but followed the model of Eq. (15) with a variance-weighted coefficient of determination (r^2) of 0.705:

$$C_{\mathrm{d}} = 6\mathrm{AR}^{-0.5} + 0.1745w\varphi^{-1}. \quad (15)$$

Models of sway inertia and drag coefficients were also developed, with variance-weighted coefficient of determination (r^2) of 0.899 and 0.884, respectively:

$$C_{\mathrm{my}} = 0.9\mathrm{AR}^{-0.5}, \quad (16)$$

$$C_{\mathrm{dy}} = (5w + 5)\mathrm{AR}^{-0.5}, \quad (17)$$

where C_{my} is the appendage sway inertia coefficient and C_{dy} is the appendage sway drag coefficient.

4.8. Centre of pressure

The spanwise centre of pressure is the point at which the sway force may be considered to act, a concept similar to that of a centre of gravity. It was determined by dividing the standard deviation of the roll moment signal by that of the sway force signal. It was found to lie between 50% and 80% of span for most conditions tested (Fig. 20). Note that errors increased with decreasing frequency and mechanical friction increased the likelihood of outlier points at low frequencies. The variation of the centre of pressure as a function of time was investigated by dividing the roll moment signal by the sway force signal at each time step.

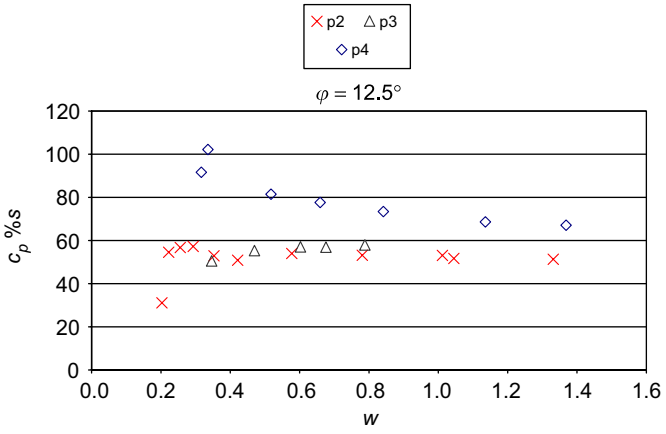

Fig. 20. Effect of plate geometry on centre of pressure.

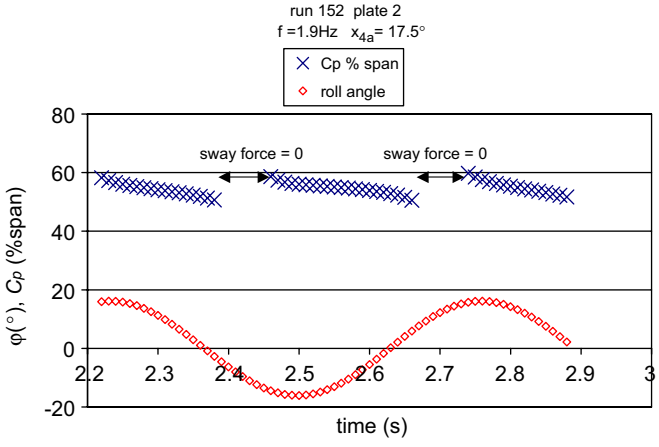

Fig. 21. Centre of pressure as a function of time.

A typical result is shown in Fig. 21, from which it is evident that the centre of pressure did not vary substantially within an oscillation. The instances within the oscillation when the sway force was very small resulted in the centre of pressure calculation being dominated by experimental error. Consequently, the data at those instances have been omitted from the figure.

5. Conclusions

For the plates used in the experiment, at Reynolds number from 2.9×10^2 to 1.8×10^5, dimensionless frequency 0.15–2.0 and roll amplitude up to 0.35 rad, and within the limits of experimental error, the following conclusions are drawn.

The two-dimensional case is not representative of three-dimensional flow conditions. There is a possible region of transitional flow for the plate in two-dimensional flow, not evidenced in the results for the plates in three-dimensional flow.

Under-plate clearance effects are small for the clearance values investigated.

The total roll moment, roll inertia, roll drag and sway force coefficients show an inverse square root relationship to aspect ratio, with a very weak dependency on oscillation frequency and angle amplitude, as given by empirical Eqs. (13)–(17).

References

Bearman, P.W., Downie, M.J., Graham, J.M.R., Obasaju, E.D., 1985. Forces on cylinders in viscous oscillatory flow at low Keulegan-Carpenter numbers. Journal of Fluid Mechanics 154, 337–356.

Chakrabarti, S.K., 1987. Hydrodynamics of Offshore Structures. Computational Mechanics, Southampton.

Keulegan, G.H., Carpenter, L.H., 1958. Forces on cylinders and plates in an oscillating fluid. Journal of Research of the National Bureau of Standards 60, 423–440.

Rae, W.H., Pope, A., 1984. Low-speed Wind Tunnel Testing. Wiley.

Ridjanovic, M., 1962. Drag coefficients of flat plates oscillating normally to their planes. Schiffsteknik 45, 13–17.

Sarpkaya, T., O'Keefe, J. L., 1995. Oscillating flow about two- and three-dimensional bilge keels. In: 14th International Conference on Offshore Mechanics and Arctic Engineering 1-A. American Society of Mechanical Engineers, Copenhagen, pp. 263–270.

Scott, J.R., 1976. Blockage correction at sub-critical speeds. Transactions Royal Institution of Naval Architects 118, 169–179.

Yeung, R., Cermelli, C., Liao, S.-W., 1997. Vorticity fields due to rolling bodies in a free surface-experiment and theory. In: 21st Symposium on Naval Hydrodynamics. National Academy Press, Trondheim, Norway, pp. 359–376.

Yeung, R.W., Liao, S.-W., Roddier, D., 1998. Hydrodynamic coefficients of rolling rectangular cylinders. International Journal of Offshore and Polar Engineering 8, 241–250.